JACS
JOURNAL OF THE AMERICAN CHEMICAL SOCIETY
Article
pubs.acs.org/JACS

Cation-Modulated Reactivity of Iridium Hydride Pincer-Crown Ether Complexes

Matthew R. Kita and Alexander J. M. Miller*

Department of Chemistry, University of North Carolina at Chapel Hill, Chapel Hill, North Carolina 27599-3290, United States

Supporting Information

ABSTRACT: Complexes of a new multidentate ligand combining a rigid, strongly donating pincer scaffold with a flexible, weakly donating aza-crown ether moiety are reported. The pincer-crown ether ligand exhibits tridentate, tetradentate, and pentadentate coordination modes. The coordination mode can be changed by Lewis base displacement of the chelating ethers, with binding equilibria dramatically altered through lithium and sodium cation−macrocycle interactions. Cation-promoted hydrogen activation was accomplished by an iridium monohydride cation ligated in a pentadentate fashion by the pincer-crown ether ligand. The rate can be controlled on the basis of the choice of cation (with lithium-containing reactions proceeding about 10 times faster than sodium-containing reactions) or on the basis of the concentration of the cation. Up to 250-fold rate enhancements in H/D exchange rates are observed when catalytic amounts of Li^+ are added.

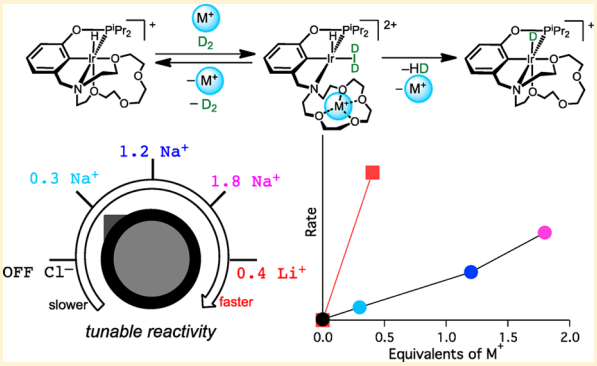

INTRODUCTION

Homogeneous catalysts featuring hemilabile ligands,[1] chelates in which one donor exhibits reversible coordination to the metal center, often display an uncommon combination of high activity and longevity.[2] The beneficial properties are ascribed to the ability of the ligand to move between a bound form that is stable toward decomposition and a dissociated form that is highly active. Unfortunately, tuning the reactivity of hemilabile catalysts is difficult: in order to change the hemilabile binding properties, a new ligand—for example, with a longer linker or different steric bulk—must be synthesized, often through arduous synthetic routes.[3−5] A strategy for controlling hemilability through noncovalent interactions could greatly facilitate catalyst tuning, minimizing synthetic effort. We report that a new pincer ligand bearing an aza-crown ether moiety enables the facile control of hemilability on the basis of alkali metal cation−macrocycle interactions.

Controlled hemilability can be classified into two categories according to the ligand dynamics, as shown in Scheme 1: (a) *static hemilability*, in which an additive switches the binding between fully associated and fully dissociated states that do not rapidly interconvert; and (b) *dynamic hemilability*, in which an additive adjusts the equilibrium constants while maintaining rapid, reversible binding.[6−8] Most responsive catalysts involve static hemilability, with discrete "on" and "off" states. Mirkin and co-workers, for example, have developed elegant supramolecular scaffolds capable of static hemilability,[6,9,10] including a Rh_2/Al scaffold that undergoes Al-catalyzed polymerization after chloride-promoted dissociation of an amine arm blocking the active site.[11] Sequestration of the chloride anion leads to reassociation of the amine and termination of catalysis.

Scheme 1

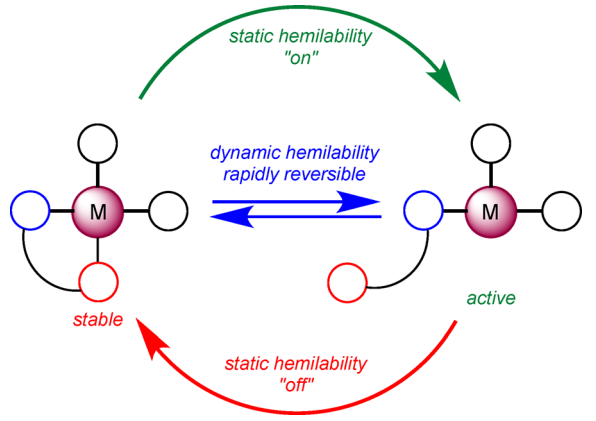

Oxidation or reduction of a pendent redox center has also been used to modulate catalytic activity through altered coordination chemistry.[12,13]

Despite the recognized role of rapid binding equilibria in bestowing hemilabile catalysts with exceptional activity and longevity,[3] strategies for inducing dynamic hemilability are lacking.[14] To this end, we targeted a ligand containing a macrocycle that could be dissociated from a transition-metal center by preferential encapsulation of a cationic additive. Rather than building a library of ligands with different structures, modulation of reactivity would be achieved by

Received: July 18, 2014
Published: October 2, 2014

   dx.doi.org/10.1021/ja507324s | J. Am. Chem. Soc. 2014, 136, 14519−14529

variation of the noncovalent interactions. Cation−macrocycle interactions offer a range of binding affinities that might allow for fine tuning of reactivity.

We describe herein flexible, cation-modulated coordination chemistry and hydrogen activation reactivity of iridium pincer-crown ether complexes. Incorporating an aza-crown ether macrocycle as the amine donor of a NCOP pincer ligand enables access to iridium complexes featuring tridentate, tetradentate, and pentadentate coordination modes. Interconversion between these binding modes is modulated by alkali metal cations that can interact with the macrocyclic ligand arm, enabling dramatic and cation-tunable acceleration of dihydrogen activation.

RESULTS AND DISCUSSION

Synthesis and Structural Characterization. Aminophosphine pincer ligands offered a convenient starting point for the installation of an aza-crown ether macrocycle balanced by strong phosphinite and phenyl anion donors. The desired aminophosphine ligand (^{15c5}NCOP^{iPr})H, containing an aza-15-crown-5 macrocycle, was synthesized according to Scheme 2.

Scheme 2

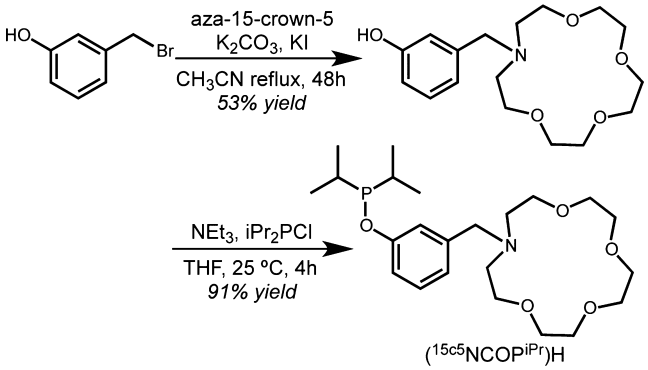

Amination of 3-bromomethylphenol[15] with aza-15-crown-5 in refluxing acetonitrile afforded the aminophenol intermediate.[16] Subsequent phosphination was accomplished using triethylamine and diisopropylchlorophosphine to yield (^{15c5}NCOP^{iPr})H as a viscous, colorless oil. Despite the structural similarity to diethylamino and morpholino NCOP ligands recently reported by Zargarian and co-workers,[17−19] a different procedure was required to install the poorly nucleophilic aza-crown amine arm.

Metalation proceeded smoothly when (^{15c5}NCOP^{iPr})H was allowed to react with [Ir(Cl)(COD)]$_2$ (COD is 1,5-cyclooctadiene) in benzene at 333 K for 12 h, forming (κ^4-^{15c5}NCOP^{iPr})Ir(H)(Cl) (**1**; Scheme 3). A single resonance was observed in the ^{31}P{^{1}H} NMR spectrum (δ 143). From the ^{1}H NMR spectrum of **1**, it was immediately apparent that the

Scheme 3

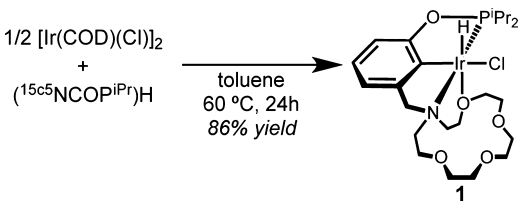

plane of symmetry containing the phenyl ring was broken, with four independent isopropyl methyl doublet of doublets apparent. The tetradentate coordination mode shown in Scheme 3 was initially suggested by the chemical shift of the hydride resonance of **1** (δ −30.9). Five-coordinate iridium hydrochloride complexes such as (POCOP)Ir(H)(Cl) (POCOP is 2,6-bis[di(*tert*-butyl)phosphinyloxy)]phenyl) are typically found far upfield (δ −40 to −42).[20] The hydride chemical shift of **1** is consistent with a weak donor *trans* to the hydride.[21] The aza-crown ether resonances are also found in unusual spectral regions, with downfield multiplets (δ 5.04, 4.94) reminiscent of Ir(III) complexes of tetradentate bis-NHC ligands with chelating alkyl ether arms.[22]

Lemon yellow single crystals of **1** suitable for an X-ray diffraction (XRD) study were obtained from a toluene solution layered with pentane at 243 K. XRD of **1** confirmed the tetradentate coordination mode, with one of the crown ether oxygen atoms bound *trans* to the hydride (Figure 1). The κ^4-

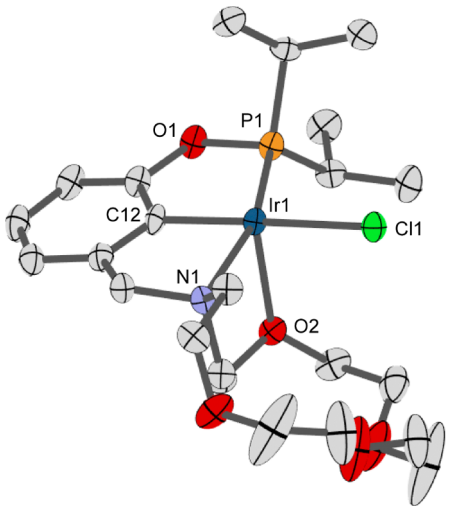

Figure 1. Structural representation of **1** with ellipsoids drawn at the 50% probability level. Hydrogen atoms are omitted for clarity. Selected distances (Å) and angles (deg): Ir1−P1 2.1825(14), Ir1−O2 2.355(4), Ir1−C12 1.979(5), Ir1−N1 2.222(5), Ir1−Cl1 2.4672(13); P1−Ir1−O2 99.63(10), O2−Ir1−Cl1 93.28(10), C12−Ir1−O2 88.23(19), C12−Ir1−Cl1 174.73(17), N1−Ir1−O2 78.46(15).

mer,fac coordination features a long Ir−O distance (2.355(4) Å) and an acute 78.5° N−Ir−O bond angle. Chelating dialkyl ether donors typically exhibit Ir−O distances in the range 2.10−2.25 Å,[23−26] although examples with longer distances have been reported.[27,28]

Addition of NaBAr$^F_4$ (Ar^F is 3,5-bis(trifluoromethyl)phenyl) to a dichloromethane solution of **1** resulted in precipitation of NaCl and formation of [(κ^5-^{15c5}NCOP^{iPr})Ir(H)][BAr$^F_4$] (**2**; Scheme 4). Subtle shifts relative to complex **1** were observed in the ^{1}H NMR spectrum (Ir−H δ −31.2), and a new singlet was observed by ^{31}P{^{1}H} NMR at δ 141.

Vapor diffusion of pentane into toluene solutions of complex **2** produced single crystals at 243 K. An XRD study confirmed chloride abstraction and revealed coordination of a second crown ether oxygen. The Ir1−O2 distance (*trans* to hydride) of 2.229(2) Å and the Ir1−O5 distance (*trans* to phenyl) of 2.277(2) Å are quite different in length but are still contracted relative to the Ir−O distance in **1**, as expected in moving to a cationic complex. The pentadentate coordination mode appears

dx.doi.org/10.1021/ja507324s | J. Am. Chem. Soc. 2014, 136, 14519−14529

Scheme 4

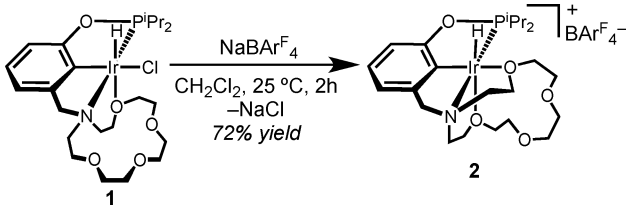

even more strained than the binding in **1**, however, with an acute N1–Ir–O5 bond angle of 76.5° (Figure 2). Complex **2** also exhibits an 11° torsion angle between the plane of the phenyl ring and the plane containing the N–Ir–P bonds (cf. 5° in **1**).

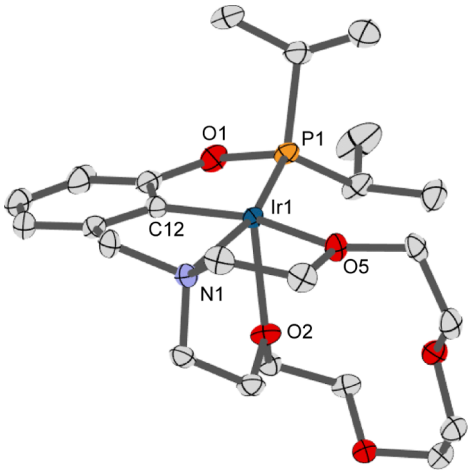

Figure 2. Structural representation of **2** with ellipsoids drawn at the 50% probability level. Hydrogen atoms and BAr$^F_4$ anion omitted for clarity. Selected distances (Å) and angles (deg): Ir1–O2 2.228(2), Ir1–O5 2.276(2), Ir1–P1 2.2115(7), Ir1–N1 2.154(3), Ir1–C12 1.958(3); O2–Ir1–O5 85.90(8), N1–Ir1–O2 78.74(9), N1–Ir1–O5 76.55(9), C12–Ir1–O5 158.00(11).

The structural features of this series highlight the flexible coordination chemistry available to pincer-crown ether complexes. While a variety of crown ether-containing ligands,[29,30] including a few pincer ligands,[31,32] have been investigated, the Lewis basic sites on the macrocycle are rarely involved in the primary coordination sphere.[33] The ability of ^{15c5}NCOP^{iPr} to provide additional donors contrasts with the reactivity of (POCOP)Ir(H)(Cl), which undergoes halide abstraction to form weakly bound solvento complexes such as [(POCOP)Ir(H)(CH_2Cl_2)]$^+$.[34]

Estimating Bond Strengths. Catalysis involving pincer-crown ether complexes would likely require initiation by displacement of one or more ether donors by a substrate. The metal–ligand bond strength of the crown ether complexes is therefore likely to be a critical factor in catalysis. Density functional theory (DFT) was used to estimate the Ir–O bond strengths of **1** and **2**. Calculations were performed using a slightly truncated form of the ligand (isopropyl groups replaced by methyl groups) and a polarized continuum model applied to simulate the CH_2Cl_2 solution unless otherwise noted (for full computational details see the Experimental Section and Supporting Information). Starting from the crystallographic coordinates, the optimized structures of **1-Me** (in the gas phase) and **2-Me** were similar to the crystallographically determined structures (all bond lengths within 0.025 Å).

To probe the dative Ir–O bond strength, the free energies of **1** and **2** were compared to those of conformations without Ir–O bonds. In all cases, the Ir–O bonds did not re-form upon minimization. Due to the flexibility of the macrocycle after decoordination, multiple conformations were calculated, with free energy variations of ~2 kcal mol^{-1} observed. Scheme 5

Scheme 5

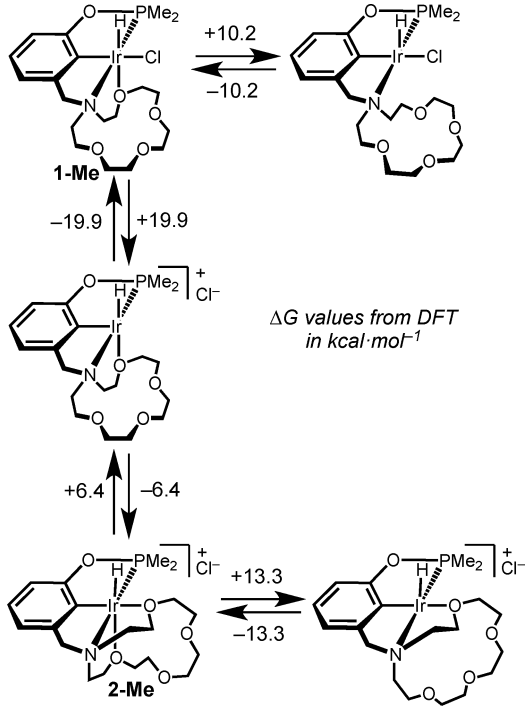

summarizes the calculated energy differences between bound and unbound forms of the ligand (lowest energy conformers given). As expected on the basis of the long bonds, dative Ir–O bonds in **1** and **2** are quite weak, with ΔG values between +6.4 and +13.3 kcal mol^{-1}. The ether ligand *trans* to the phenyl ring is thermodynamically the easiest Ir–O bond to break, consistent with crystallographically apparent strain. The Ir–O bonds in **1** and **2** appear to be substantially weaker than those of related hemilabile systems involving Ir–N bonds (21–28 kcal mol^{-1} dissociation energy).[35] The activation energies of hemilabile binding of phosphinoethers to late transition metals are typically 11–16 kcal mol^{-1}.[3] Complexes **1** and **2** are related by chloride dissociation. While removing chloride from **1** without any macrocycle rearrangement is quite unfavorable, subsequent chelation to pentadentate binding provides an overall ΔG = 13.5 kcal mol^{-1}—only slightly more unfavorable than ether dissociation in some cases.

Reactivity with Lewis Bases. The relative metal–ligand bond strengths in complexes **1** and **2** can be assessed experimentally through reactivity studies with nucleophiles: weak Ir–O bonds will be displaced by weakly Lewis basic donors; strong Ir–O bonds will only be displaced by strongly Lewis basic donors. The resulting products would possess the typical tridentate pincer geometry.

Weakly basic THF was investigated first. Addition of up to 300 equiv of THF to a $CDCl_3$ solution of **2** did not result in any new species visible by ^{1}H or ^{31}P{^{1}H} NMR spectroscopy.

dx.doi.org/10.1021/ja507324s | J. Am. Chem. Soc. 2014, 136, 14519–14529

THF is apparently too poor a ligand to displace the chelating ether donors in **2**.

On the other hand, addition of $[Bu_4N][Cl]$ to **1** led to a mixture containing unreacted **1** along with a new species assigned as $[(\kappa^3\text{-}^{15c5}NCOP^{iPr})Ir(H)(Cl)_2]^-$ (**4**). The hydride resonance of **4** (δ −24.17) indicates replacement of the ether ligand *trans* to the hydride site with a stronger donor.[20] When the analogous reaction with $[Bu_4N][Br]$ was carried out, we were surprised to observe *six* species by NMR spectroscopy. The hydride signals of these six species were observed as closely spaced pairs in three different regions (Figure S16 in the Supporting Information), prompting the following assignments: **1**, the bromo analogue of **1**, $(\kappa^4\text{-}^{15c5}NCOP^{iPr})Ir(H)(Br)$, dichloride **4**, the dibromide analogue of **4**, $[(\kappa^3\text{-}^{15c5}NCOP^{iPr})Ir(H)(Br)_2]^-$, and the two possible bromochloride anion isomers. The presence of all possible halide species indicates that halide substitution is facile in chlorinated solvents.

The macrocyclic ether ligand of hydrochloride **1** is also readily displaced by CH_3CN, but the crown ether signals of **1** broadened substantially during addition, suggesting an additional fluxional process. When the temperature was lowered to 273 K, the resonances sharpened and an additional species appeared. The two new species were hypothesized to be the stereoisomers of $(\kappa^3\text{-}^{15c5}NCOP^{iPr})Ir(H)(Cl)(NCCH_3)$ with *cis*-hydrochloride (**3**) and *trans*-hydrochloride (**3′**) arrangements.[36,37] The species were distinguished using an isotopic labeling experiment wherein $^{15}NCCH_3$ was added to **1**. As shown in Figure 3, the broad hydride resonance at δ −21.9, previously observed as a doublet ($^2J_{PH}$ = 25.8 Hz), sharpened into a triplet ($^2J_{PH}$ = $^2J_{NH}$ = 26.3 Hz) upon cooling. The observed coupling constant assigns this minor product as **3**, with the hydride *trans* to $^{15}NCCH_3$. The major product observed at room temperature thus is *not* **3**, as expected, but rather the *trans*-hydrochloride isomer **3′**. Consistent with this assignment, the hydride resonance of **3′** (δ −23.05) exhibited weaker N−H coupling and remained a doublet in the labeling experiment ($^2J_{PH}$ = 23.5 Hz, $^2J_{NH}$ < 2 Hz).

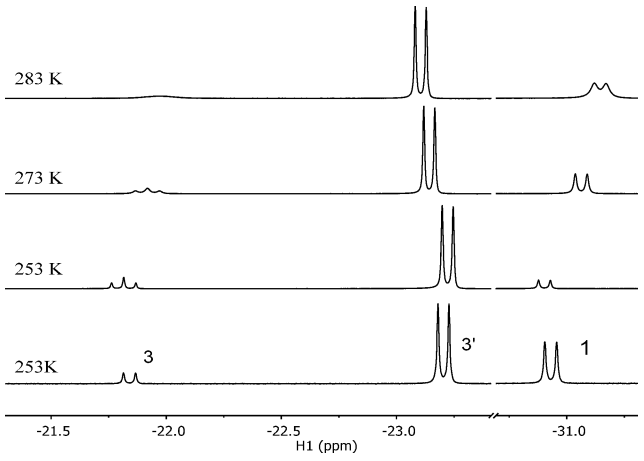

Figure 3. ^1H NMR spectra (hydride region) after addition of $^{15}NCCH_3$ to **1**, at 283, 273, and 253 K. The bottom spectrum shows the mixture after addition of unlabeled CH_3CN to **1** at 253 K.

A plausible mechanism for the formation of **3** and **3′** from **1** that is consistent with the experimental observations is shown in Scheme 6. The roughly simultaneous broadening of signals for **1**, **3**, and free CH_3CN indicates that **1** and **3** are in dynamic equilibrium on the time scale of NMR spectral acquisition.

Scheme 6

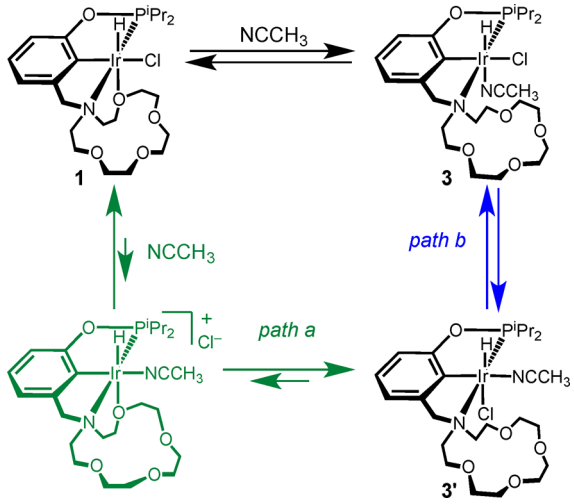

Isomer **3′** could be formed by one of two slower processes, as shown in Scheme 6: via an unfavorable (and unobserved) cationic intermediate (path a) or via **3** followed by isomerization (path b). The rapid scrambling observed upon addition of $[Bu_4N][Br]$ to **1** and DFT calculations suggest that path a is possible.

Thermodynamic parameters for acetonitrile binding to **1** were extracted on the basis of variable-temperature (VT) NMR experiments using a van 't Hoff analysis (Figure 4A). Thermodynamic parameters for the conversion of **1** to **3** were as follows: ΔH° = −8.67 kcal mol^{-1}, ΔS° = −26.6 cal mol^{-1} K^{-1}. The thermodynamic parameters for the conversion of **1** to **3′** were similar: ΔH° = −8.50 kcal mol^{-1}, ΔS° = −22.4 cal mol^{-1} K^{-1}. The large negative entropies of reaction are consistent with adduct formation being involved in each equilibrium.

The CH_3CN binding process studied by VT NMR spectroscopy was also examined computationally. The conversion of **1-Me** to the *cis*-hydrochloride isomer **3-Me** was calculated to be uphill by ΔG = 9.0 kcal mol^{-1}, with **3′-Me** being more stable than **3-Me** ($\Delta\Delta G$ = −0.5 kcal mol^{-1} at 298 K). While the calculations reproduce the relative energies of **3′** and **3** ($\Delta\Delta G^\circ$ = −1.0 kcal mol^{-1} on the basis of NMR data), the overall free energy values do not agree very well. Noncovalent interactions with CH_2Cl_2 or CH_3CN may be involved, as weak H-bonding interactions have been shown (in experiment and theory) to be enthalpically favorable by 5−20 kcal mol^{-1}.[38−40] More detailed computational models, accounting for all noncovalent interactions, are needed in the future.[41]

The pentadentate-coordinated complex **2** reacts with acetonitrile as shown in Scheme 7. Addition of up to 1 equiv of CH_3CN gave smooth, complete conversion to $[(\kappa^4\text{-}^{15c5}NCOP^{iPr})Ir(H)(NCCH_3)]^+$ (**5**) (the equilibrium constant could not be measured). Complex **5** has a *cis*-hydronitrile geometry, as evidenced by the small (0.35 ppm) upfield shift of the hydride resonance consistent with an ether ligand remaining *trans* to hydride. Accordingly, when the $^{15}NCCH_3$ analogue of **5** was formed, no N−H coupling was observed. The preference for substitution *trans* to phenyl is consistent with the longer, more strained Ir−O bond being more weakly bound.

dx.doi.org/10.1021/ja507324s | J. Am. Chem. Soc. 2014, 136, 14519−14529

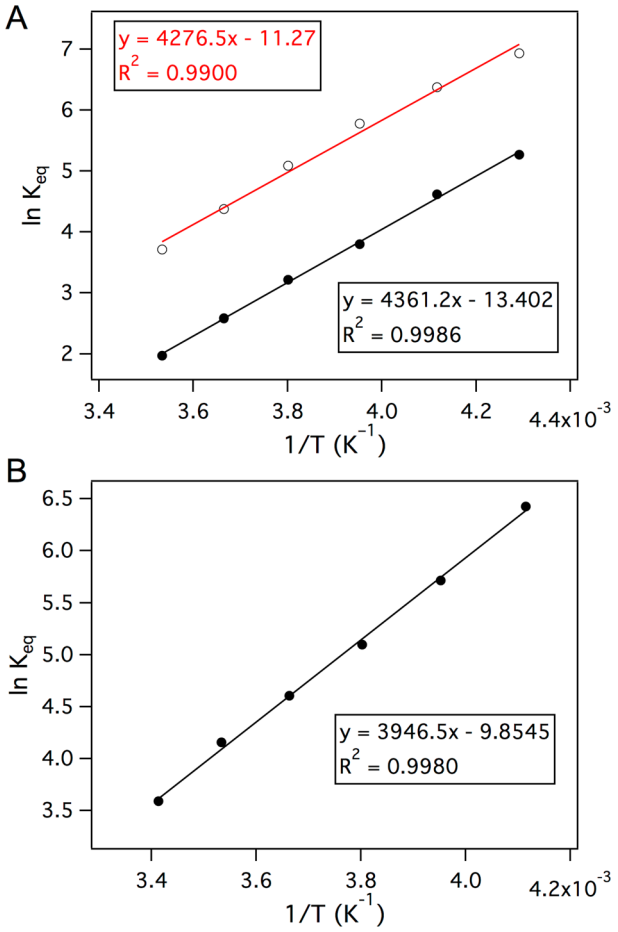

Figure 4. Van 't Hoff analysis of (A) adduct formation between **1** and CH_3CN to produce **3** (filled circles with black linear fit) and **3′** (empty circles with red linear fit) and (B) adduct formation between **5** and CH_3CN to produce **6** (filled circles with black linear fit).

Addition of more CH_3CN to **5** engaged an equilibrium among **5**, $[(\kappa^3\text{-}^{15c5}NCOP^{iPr})Ir(H)(NCCH_3)_2]^+$ (**6**), and free CH_3CN (Scheme 7): K_{eq} = 34.0 M^{-1} at 298 K. Thermodynamic parameters for the second step of Scheme 7 were obtained by van 't Hoff analysis (Figure 4B): $\Delta H^\circ = -7.8$ kcal mol^{-1} and $\Delta S^\circ = -19.6$ cal mol^{-1} K^{-1}.

DFT calculations are qualitatively consistent with the observed adduct formation in **2**. Reaction of **2-Me** with 1 equiv of CH_3CN to form **5-Me** was calculated to be favorable ($\Delta G = -6.6$ kcal mol^{-1}). Formation of the other (unobserved) isomer of **5-Me** was calculated to be unfavorable with respect to **2-Me** and free CH_3CN ($\Delta G = +4.7$ kcal mol^{-1}). Reaction of **5-Me** with another 1 equiv of CH_3CN to generate **6-Me** is calculated to be close to thermoneutral ($\Delta G = +1.9$ kcal mol^{-1}), consistent with the observed equilibrium.

The binding studies confirm that appropriate ligands (or substrates) can displace the macrocyclic chelate(s) to form the typical tridentate pincer coordination mode. These processes can be rapid, with fluxional NMR processes observed in some cases. Interestingly, both adduct formations are chemically reversible: for example, exposing complex **6** to vacuum led to re-formation of pentadentate cation **2**.

Cation-Modulated Binding Equilibria. The pincer-crown ether ligand was designed to promote cation−macrocycle interactions. Cation intercalation seemed likely to perturb the ligand substitutions discussed above, since the resulting dissociated macrocycle would be free to interact with s-block cations. Cation−macrocycle interactions were therefore targeted in subsequent studies. Lithium and sodium salts of the weakly coordinating, lipophilic BAr^F_4 anion were used, on the basis of early indications that triflato ions bind Ir (Figure S30 in the Supporting Information).[42]

Addition of $LiBAr^F_4$ or $NaBAr^F_4$ to CD_2Cl_2 solutions of **2** (containing 125 mM Et_2O for improved solubility) resulted in no observable shifts in the resonances of **2**. Whether or not the macrocyclic ligands are dissociating, this indicates that any equilibrium formation of low-coordinate or solvento species is strongly disfavored under these conditions.

Alkali metal cations present in solution dramatically perturb adduct-forming equilibria involving **2** (Scheme 8). Whereas adduct formation between CH_3CN and **2** establishes equilibrium in the absence of salts (Scheme 7), the reaction is irreversible in the presence of $NaBAr^F_4$ (no free CH_3CN was observed, precluding equilibrium measurements). Even with less than 2 equiv of CH_3CN, the bis-nitrile complex is the major product under these conditions. Attempts to reverse the reaction under reduced pressure (solids exposed to vacuum for 11 h) were unsuccessful, in sharply contrast with the facile removal of CH_3CN ligands from **6** in the absence of salts. Analogous behavior was observed upon addition of CH_3CN to solutions of **2** containing $LiBAr^F_4$.

Perturbation of equilibria is attributed to cation−crown interactions. Figure 5 shows the effect of adding increasing amounts of Na^+ to an equilibrium mixture of CH_3CN, **5**, and **6**. The hydride resonance of **5** shows no change in chemical shift with increasing amounts of Na^+. The hydride resonance of **6**, however, broadens and shifts upfield, and another hydride resonance of similar chemical shift appears as more Na^+ is added. The cation-dependent chemical shift indicates rapid reversible adduct formation between Na^+ and **6**, made possible when the tridentate binding mode of the pincer-crown ligand is accessed (Scheme 8). The products must be closely related, as they feature overlapping hydride resonances and two sets of CH_3CN methyl resonances. The appearance of an extra set of peaks for the BAr^F_4 anion is consistent with different ion-pairing or aggregation states mediated by Na^+.[43−45] The data indicate that stronger cation−crown interactions are present in the tridentate coordination mode of **6** than in the tetradentate

Scheme 7

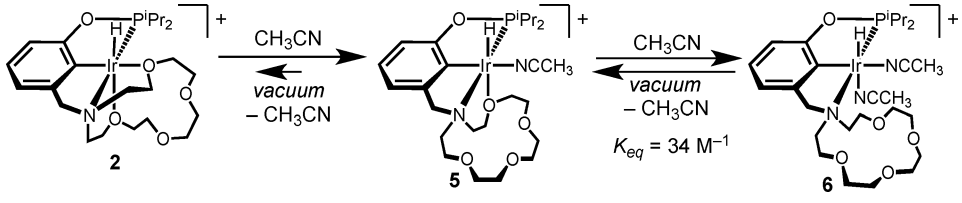

dx.doi.org/10.1021/ja507324s | J. Am. Chem. Soc. 2014, 136, 14519−14529

Scheme 8

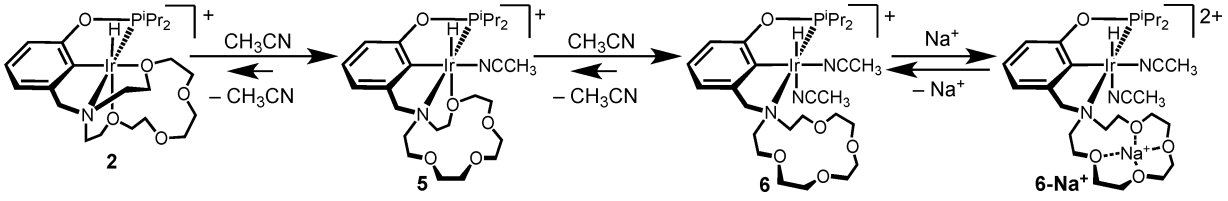

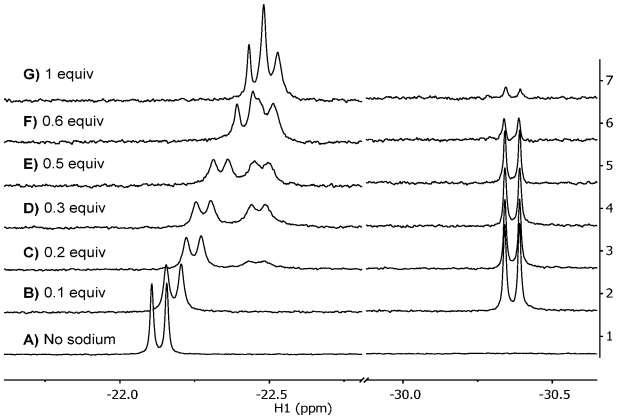

Figure 5. ^{1}H NMR spectra (hydride region) showing the reaction of 9.3 mM **2** in $CDCl_3$ (containing 185 mM Et_2O) with CH_3CN under various conditions: (A) addition of 192 equiv of CH_3CN to form complex **6** (δ −22.13); (B−G) addition of 3 equiv of CH_3CN to establish an equilibrium mixture of **5** (δ −30.37) and **6**, followed by increasing amounts of Na^+ as indicated.

coordination mode of **5** (wherein no interaction with Na^+ is apparent by NMR spectroscopy). In CD_3CN, only one hydride resonance is observed, and similar sodium-dependent changes in chemical shift are observed by ^{1}H and ^{13}C{^{1}H} NMR spectroscopy (Figures S42 and S43, Supporting Information).

Cation-Accelerated Dihydrogen Splitting. Weak donors such as THF are unable to displace the chelating ether ligands of cationic complex **2**. The pincer-crown ether ligand therefore has the potential to act as a "gate" for substrate binding for catalytic reactions. A weakly coordinating substrate would not readily undergo substitution reactions at the coordinatively saturated metal center. An appropriate cation could, however, alter the substrate binding constants, effectively opening the gate and initiating catalysis.

To test this hypothesis, we targeted the very weakly coordinating dihydrogen ligand,[46,47] the binding and activation of which is critical to numerous catalytic reactions. These reactions were carried out in chlorinated solvents with small amounts of diethyl ether to ensure full solubility of the alkali metal salts. Exposure of CD_2Cl_2 solutions containing 6.25 mM hydride **2** and 125 mM Et_2O to an atmosphere of D_2 gas resulted in slow H/D exchange (Scheme 9). The hydride signal of **2** exhibited exponential decay kinetics under 1 atm of D_2

Scheme 9

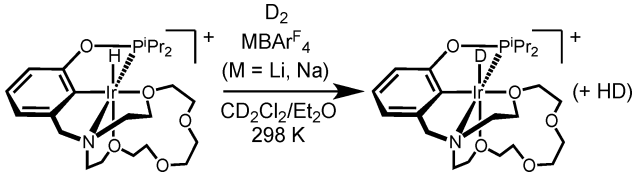

(k_{obs} = 1.2 × 10^{-6} s^{-1}, $t_{1/2}$ = 160 h), indicating a process that is first order in **2**. During the reaction, only the ^{1}H NMR resonance for the Ir−H changed, gradually disappearing. By ^{31}P{^{1}H} NMR spectroscopy, however, two distinct resonances were observed, with the signal for **2** (δ 140.98) being consumed with simultaneous formation of a new resonance at nearly identical chemical shift (δ 141.26). The similarity in spectral signatures, along with the presence of a deuteride signal at δ −29.7 in the ^{2}H NMR spectrum, confirm that the product is [(κ^5-^{15c5}NCOP^{iPr})Ir(D)][BAr$^F_4$] (**2-D**). This rate of deuterium incorporation is much slower than that for [(POCOP)Ir(H)(D$_2$)]$^+$, which undergoes exchange within seconds.[48] The additional ether donors in **2** prohibit observation of a hydrido−dihydrogen complex and substantially hinder the reaction.

The reaction was repeated under identical conditions but in the presence of LiBAr$^F_4$ and NaBAr$^F_4$ additives. In the presence of just 0.3 equiv of Na^+, Ir−H was converted to Ir−D with the rate constant k_{obs} = 2.4 × 10^{-5} s^{-1} ($t_{1/2}$ = 483 min). It is noteworthy that this dramatic 20-fold rate enhancement occurs with a substoichiometric quantity of Na^+ in solution. Even faster rates of D_2 cleavage were observed when 0.4 equiv of LiBAr$^F_4$ was added, with an observed rate constant of 2.8 × 10^{-4} s^{-1} ($t_{1/2}$ = 40 min), indicating a roughly 250-fold rate acceleration. The ability to modulate the reaction rate on the basis of the choice of alkali metal salt is particularly exciting: small differences in binding energies (<1 kcal mol^{-1} in many examples involving Li^+/Na^+ adducts with 12-crown-4) result in rates that differ by 1 order of magnitude.[49,50] The catalyst is "selective" for lithium promotion over sodium promotion, presumably on the basis of the macrocycle size. With only four donors (at most) available to interact with the s-block metal ion, interactions with smaller cations such as Li^+ may be favored.

Additional NaBAr$^F_4$ leads to even faster conversion to the Ir−D species **2-D**, as shown in Figure 6B. Moving from 0.3 equiv of Na^+ to 2.5 equiv of Na^+, the reaction accelerates markedly (the half-life decreases from 483 to 36 min). Thus, the reaction rate can be tuned over 2 orders of magnitude either by changing the identity of the cation (Li^+ vs Na^+) or by adjusting the concentration of a particular cation (as shown in the experiments varying [Na^+]). Interestingly, the plot of k_{obs} vs concentration of Na^+ is nonlinear (Figure 6B), with faster than expected rates at higher concentrations of Na^+. This may reflect modest quenching of the Lewis acidity of Na^+ by Et_2O. At low [Na^+], more Et_2O relative to Na^+ will be present, which can donate to Na^+ and moderate the Lewis acidity. At high [Na^+], on the other hand, less Et_2O is present relative to Na^+, enhancing the ability of Na^+ to interact with the macrocylic pincer ligand. This theory is buttressed by the observation that the ^{1}H NMR resonances of Et_2O shift as a function of [Na^+], indicating rapid adduct formation equilibrium.

A plausible mechanism involving tunable dynamic hemilability is proposed to account for the cation-dependent

dx.doi.org/10.1021/ja507324s | J. Am. Chem. Soc. 2014, 136, 14519−14529

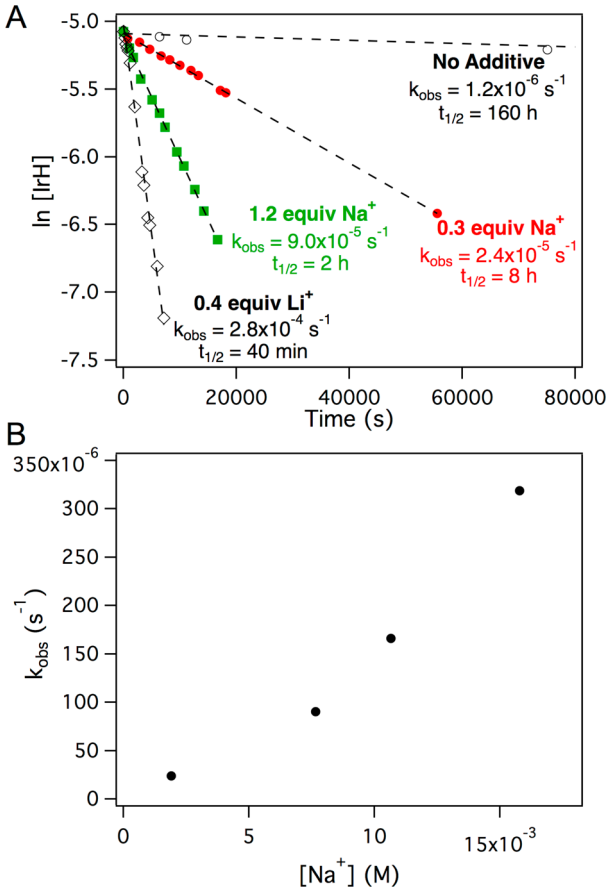

Figure 6. (A) Plot of the natural log of concentration of hydride **2** versus time during the reaction with 1 atm of D_2. The reaction was run with no added salts (empty cirlces), 0.3 equiv of $NaBAr^F_4$ (red circles), 1.2 equiv of $NaBAr^F_4$ (green sqaures), and 0.4 equiv of $LiBAr^F_4$ (empty diamonds). Linear fits are given by dashed lines. (B) Plot of observed first-order rate constant versus concentration of Na^+. Conditions: 6.25 mM **2**, 125 mM Et_2O, CD_2Cl_2, 298 K. For full details, see the Supporting Information.

conversion of **2** to **2-D**, as shown in Scheme 10. We propose that intercalation of lithium or sodium ion into the macrocycle stabilizes a reactive deuterium σ complex, which then undergoes H/D exchange followed by release of the cation and HD gas. The observed influence of Li^+ and Na^+ on the

Scheme 10

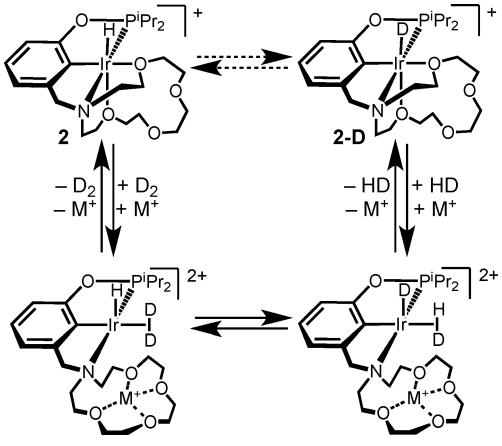

equilibrium of acetonitrile substitution provides a basis for the proposed stabilization of the dihydrogen complex. No intermediates were observed during in situ ^1H NMR spectroscopic monitoring, however, and no shifts in the resonances of **2** were observed with increasing amounts of Na^+ (although the resonances of Et_2O did shift; Figure S38 in the Supporting Information). These observations suggest that equilibrium dissociation of the macrocycle is kinetically accessible but thermodynamically unfavorable—as is typical for hemilabile catalysts.[2,3] The more dramatic rate enhancement by Li^+ is attributed to larger shifts in the equilibrium constants due to stronger interactions with the four ether donors of the pendant macrocycle.

Following complete deuteration, hydride **2** could be reformed by placing deuteride **2-D** under 1 atm of H_2. For reactions carried out in the presence of Li^+ and Na^+ (cf. Figure 6), hydride **2** reacted with D_2 1.6–2.0 times faster than deuteride **2-D** reacted with H_2 (Figures S39 and S40, Supporting Information). These values reflect a primary isotope effect, but a detailed interpretation is complicated.[51] For comparison, (POCOP)Ir(H)(H_2) undergoes site exchange ~6 times faster than (POCOP)Ir(D)(D_2).[48]

The reaction can also be carried out in CD_2Cl_2 or $CDCl_3$ without added Et_2O. Similar rate enhancements were observed in the presence of $NaBAr^F_4$ ($t_{1/2}$ = 14 h) and $LiBAr^F_4$ ($t_{1/2}$ = 11.9 min), which is remarkable given the almost complete insolubility of the BAr^F_4 salts under these conditions (on the basis of relative integration of the Ar^F protons).

The reaction rate can be slowed by the removal of Na^+ from solution. Figure 7 shows the conversion of **2** as it reacts rapidly

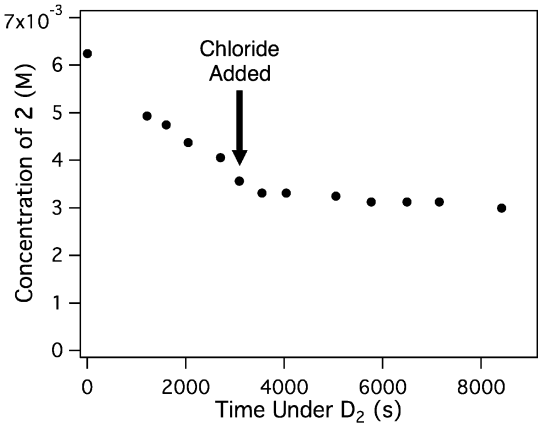

Figure 7. Progress of the reaction of **2** with 1 atm of D_2 in the presence of $NaBAr^F_4$ (1.9 equiv) hindered by the addition of $[Bu_4N][Cl]$ (1.8 equiv) after 3000 s. Conditions: 6.25 mM **2**, 125 mM Et_2O, CD_2Cl_2, 298 K.

with D_2 in the presence of 1.9 equiv of $NaBAr^F_4$. The reaction was allowed to proceed to ~60% conversion, at which time the tube was degassed and 1.8 equiv of $[Bu_4N][Cl]$ was added. After the D_2 atmosphere was restored, the reaction proceeded—but at a rate 5 times slower than that before chloride addition. The reduction in rate and the observed white precipitate suggest that Na^+ was removed from solution as insoluble NaCl. The rate after chloride addition is consistent with the presence of only a small amount of residual Na^+. The ability to speed up or slow down a reaction through sequential addition of Na^+ and Cl^- is reminiscent of Mirkin's catalysis involving static hemilability, but the roles of Na^+ and Cl^- are

dx.doi.org/10.1021/ja507324s | J. Am. Chem. Soc. 2014, 136, 14519–14529

reversed: previous systems rely on Cl^- for activation and Na^+ for deactivation, whereas here Na^+ is the activating reagent and Cl^- deactivates the reaction.[11]

Most previous reports on controlling hemilability have focused on switchable catalysis using static hemilability.[6,10] These catalysts are either fully active or fully inactive. In contrast, the kinetics of hydrogen activation by **2** reveal the ability of cation−crown interactions to smoothly tune the reaction rate on the basis of the identity and concentration of the ion. Even with excess cation, the only observed species is a stabilized form of the complex, suggesting that the benefits of dynamic hemilability might be retained in catalysis (whereas a catalyst featuring static hemilability, with a fully dissociated ligand, might be prone to decomposition). The observation that Li^+ and Na^+ exhibit different levels of activity is particularly intriguing, suggesting that matching the cation to the macrocycle can tune catalyst activity in a highly controlled fashion. The weak cation−macrocycle interactions are well matched to the energy regimes found in catalysis, where small energy differences give large differences in activity or selectivity.

CONCLUSIONS

A series of iridium complexes supported by a new pincer-crown ether ligand exhibit remarkable flexibility in coordination chemistry, with tridentate, tetradentate, and pentadentate coordination modes being observed. The addition of weak ligands can selectively displace the ether donors, and further modulation in the binding energetics is achieved through alkali metal cation interactions with the crown ether. The cation-triggered ligand binding was used to develop a cation-promoted hydrogen activation reaction, monitored by H/D exchange. Dihydrogen activation is proposed to proceed by a cation-modulated *dynamic hemilability* mechanism. The reaction rate can be tuned over 2 orders of magnitude on the basis of the identity and concentration of the cation, but significantly the resting state remains the stable, coordinatively saturated form of the complex.

EXPERIMENTAL SECTION

General Considerations. All compounds were manipulated using standard vacuum line or Schlenk techniques or in a glovebox under a nitrogen atmosphere. NMR scale reaction mixtures were prepared under nitrogen in a glovebox and kept in Teflon-sealed tubes. Under standard glovebox operating conditions, pentane, diethyl ether, benzene, toluene, and tetrahydrofuran were used without purging, such that traces of those solvents were present in the atmosphere and in the solvent bottles. ^{1}H, ^{31}P, ^{19}F, and ^{13}C NMR spectra were recorded on 400, 500, and 600 MHz spectrometers. NMR characterization data are reported at 298 K, unless specified otherwise. All NMR solvents and isotopically labeled reagents were purchased from Cambridge Isotope Laboratories, Inc. Benzene-d_6 (C_6D_6), chloroform-d ($CDCl_3$), and methylene chloride-d_2 (CD_2Cl_2) were freeze−pump−thaw degassed three times before drying by passage through a small column of activated alumina. Tetrahydrofuran-d_8 (THF-d_8) was purchased in a sealed ampule, which was broken under an N_2 atmosphere before filtration through activated alumina. Chemical shifts for ^{1}H and ^{13}C NMR spectra are reported in ppm relative to residual proteo solvent impurity.[52] ^{31}P resonances are reported relative to 85% H_3PO_4 external standard (0 ppm). ^{19}F resonances are reported relative to 0.05% trifluorotoluene ($C_6H_5CF_3$) in $CDCl_3$ as an external standard (−63.72 ppm). $NaBAr^F{}_4$,[38] $[H\cdot(OEt_2)_2][BAr^F{}_4]$,[53] and *m*-(bromomethyl)phenol[15] were synthesized according to literature procedures. All other reagents were commercially available and were used without further purification. Elemental analyses were performed by Atlantic Microlabs (Norcross, GA) and Robertson Microlit Laboratories (Ledgewood, NJ).

Single-crystal X-ray diffraction (XRD) data for all complexes were collected on a Bruker Smart Apex-II diffractometer at 100 ± 2 K with Cu Kα radiation (λ = 1.54175 Å). Integration of diffraction profiles was done using the program SAINT. Absorption corrections were applied using TWINABS or SADABS. Structures for complex **1** and **2** were solved using direct methods and refined using the XL refinement package via least squares.[54] Hydrogen atoms were generated theoretically and refined isotropically with fixed thermal factors.

High-resolution mass spectrometry (HRMS) (resolution 100000, mass error ≤1 ppm) measurements were performed in positive ion mode on a Thermo Scientific LTQ-FT (Waltham, MA).

Synthesis of *m*-(Aza-15-crown-5)methylphenol. A 250 mL Schlenk flask was charged with 0.7943 g (4.077 mmol) of aza-15-crown-5, 0.567 g (4.103 mmol) of K_2CO_3, 0.690 g (4.096 mmol) of KI, 0.762 g (4.103 mmol) of *m*-(bromomethyl)phenol, and 100 mL of acetonitrile. The solution was degassed by sparging with nitrogen for 20 min. A reflux condenser was attached under N_2 counter flow, and the reaction mixture was refluxed for 48 h. The reaction mixture was cooled to room temperature and filtered in air, and the remaining solids were washed with acetonitrile. Solvent was removed from the filtrate by rotary evaporation to yield a white powder. This powder was dissolved in water and extracted with chloroform to remove any salts trapped in the macrocycle. The organic fractions were combined and concentrated by rotary evaporation to afford 0.604 g (53% yield) of *m*-(aza-15-crown-5)methylphenol as a brown oil. ^{1}H NMR (400 MHz, acetone-d_6): δ 7.10 (t, J = 7.8, 1H), 6.93 (s, 1H), 6.71 (dd, J = 8.0, 2.6, 2H), 3.67 (d, J = 3.0, 8H), 3.66−3.58 (m, 10H), 2.70 (t, J = 5.1, 4H). ^{1}H NMR (600 MHz, benzene-d_6): δ 7.86 (dd, J = 2.7, 1.4 Hz, 1H), 7.16 (t, J = 7.6 Hz, 1H), 7.02 (dd, J = 8.0, 2.6 Hz, 1H), 6.72 (dt, J = 7.5, 1.1 Hz, 1H), 3.53 (s, 2H), 3.43−3.39 (m, 8H), 3.36−3.33 (m, 4H), 3.32−3.28 (m, 4H), 2.57−2.53 (m, 4H). ^{13}C{^{1}H} NMR (151 MHz, benzene-d_6): δ 158.40, 143.13, 118.32, 116.48, 113.96, 71.28, 70.81, 70.17, 69.95, 59.86, 56.75. HRMS: m/z calcd for $C_{17}H_{28}O_5N$ ($M + H^+$) 326.19620, found m/z 326.19616.

Synthesis of (^{15c5}NCOP^{iPr})H. In a glovebox, a 20 mL scintillation vial was charged with 0.134 g (0.412 mmol) of *m*-(aza-15-crown-5)methylphenol and 10 mL of THF. To the clear, colorless solution was added 64 μL (0.454 mmol) of triethylamine dropwise by syringe with stirring. After the mixture was stirred for 15 min, 65 μL (0.412 mmol) of diisopropylchlorophosphine was added dropwise by syringe with continued stirring. After chlorophosphine addition, the solution developed a light yellow-brown color. The solution was stirred for 4 h, during which time a white precipitate formed. Removal of solvents in vacuo yielded a mixture of an oil and a white powder. The oil was extracted with ether (5 × 2 mL) and filtered. The ether was removed in vacuo to yield 0.166 g (91% yield) of (^{15c5}NCOP^{iPr})H as a colorless oil. ^{1}H NMR (400 MHz, chloroform-d): δ 7.16 (t, J = 7.8 Hz, 1H), 7.05 (d, J = 2.0 Hz, 1H), 6.94 (dd, J = 11.0, 7.9 Hz, 2H), 3.72−3.58 (m, 16H), 2.79 (t, J = 6.1 Hz, 4H), 1.91 (sept d, J = 7.1, 2.4 Hz, 2H), 1.27−0.99 (m, 12H). ^{13}C NMR (151 MHz, chloroform-d): δ 159.45 (d, $^2J_{P-C}$ = 8.4 Hz), 141.51, 129.10, 122.17, 119.04 (d, $^3J_{P-C}$ = 9.6 Hz), 117.09 (d, $^3J_{P-C}$ = 10.9 Hz), 71.16, 70.72, 70.36, 70.27, 60.79, 54.43, 28.45 (d, $^1J_{P-C}$ = 17.4 Hz), 17.93 (d, $^2J_{P-C}$ = 20.1 Hz), 17.20 (d, $^2J_{P-C}$ = 8.4 Hz). ^{31}P{^{1}H} NMR (162 MHz, chloroform-d): δ 149.86. HRMS: m/z calcd for $C_{23}H_{41}NO_5P$ ($M + H^+$) 442.27169, found m/z 442.27188.

Synthesis of (^{15c5}NCOP^{iPr})Ir(H)(Cl) (1). In a glovebox, 198.5 mg (0.4496 mmol) of (^{15c5}NCOP^{iPr})H, 133.3 mg (0.1980 mmol) of $[Ir(Cl)(COD)]_2$, and 15 mL of toluene were added to a 100 mL Teflon-sealed pressure vessel. The reaction flask was removed from the glovebox and heated to 333 K for 12 h. After the mixture was cooled to room temperature, the volatiles were removed in vacuo to afford green-yellow solids. The crude mixture was solubilized in a minimal amount of toluene and layered with pentane to crash out yellow crystals of (^{15c5}NCOP^{iPr})Ir(H)(Cl) (**1**). The solvent was decanted away, and the crystals were rinsed with pentane (3 × 4 mL). The crystals were dried in vacuo to afford 228.2 mg (86% yield) of yellow crystalline **1**. Crystals suitable for X-ray diffraction were grown by

dx.doi.org/10.1021/ja507324s | J. Am. Chem. Soc. 2014, 136, 14519−14529

vapor diffusion of pentane into a concentrated solution of the product in toluene at 243 K. ^{1}H NMR (600 MHz, chloroform-*d*): δ 6.69 (t, J = 7.7 Hz, 1H), 6.56 (d, J = 7.9 Hz, 1H), 6.53 (d, J = 7.5 Hz, 1H), 5.04 (t, J = 10.6 Hz, 1H), 4.94 (dd, J = 15.2, 11.3 Hz, 1H), 4.50−4.37 (m, 2H), 4.28 (dd, J = 13.9, 11.1 Hz, 1H), 4.15−4.02 (m, 2H), 3.94 (dd, J = 13.4, 10.0 Hz, 1H), 3.91−3.59 (m, 10H), 3.52 (dd, J = 11.9, 6.4 Hz, 1H), 3.45 (dd, J = 10.5, 6.4 Hz, 1H), 3.36 (d, J = 11.2 Hz, 1H), 3.29 (dd, J = 15.6, 3.1 Hz, 1H), 2.99 (dd, J = 14.6, 3.6 Hz, 1H), 2.60−2.47 (m, 1H), 1.39 (ddd, J = 33.7, 15.2, 7.1 Hz, 6H), 1.18 (dd, J = 18.9, 7.0 Hz, 3H), 0.88 (dd, J = 15.4, 7.0 Hz, 4H), −31.25 (d, J = 26 Hz). ^{1}H NMR (600 MHz, benzene-d_6): δ 6.90 (d, J = 7.9 Hz, 1H), 6.84 (t, J = 7.7 Hz, 1H), 6.47 (d, J = 7.3 Hz, 1H), 5.28 (t, J = 10.4 Hz, 1H), 5.07 (dd, J = 15.4, 11.1 Hz, 1H), 4.10 (t, J = 12.6 Hz, 1H), 3.95 (d, J = 14.7 Hz, 2H), 3.82 (dd, J = 15.3, 3.0 Hz, 1H), 3.75 (dd, J = 13.7, 11.1 Hz, 1H), 3.64 (t, J = 12.1 Hz, 1H), 3.62−3.43 (m, 5H), 3.39 (dd, J = 10.8, 7.4 Hz, 1H), 3.28−3.13 (m, 3H), 3.09−2.93 (m, 3H), 2.73 (dd, J = 14.4, 3.9 Hz, 1H), 2.48 (ddd, J = 14.5, 11.7, 7.1 Hz, 1H), 2.23 (dp, J = 13.6, 6.9 Hz, 1H), 1.43 (dd, J = 16.6, 7.6 Hz, 3H), 1.38−1.24 (m, 6H), 1.01 (dd, J = 15.4, 6.8 Hz, 3H), −30.93 (d, J = 26.3 Hz, 1H). ^{13}C{^{1}H} NMR (126 MHz, benzene-d_6): δ 163.97 (d, J = 3.7 Hz), 148.84 (d, J = 3.2 Hz), 135.94 (d, J = 4.6 Hz), 122.96, 113.60, 107.71 (d, J = 11.3 Hz), 76.29, 73.44, 73.11, 72.93, 70.70, 70.54, 69.33, 68.87, 67.26 (d, J = 2.4 Hz), 65.01 (d, J = 2.2 Hz), 63.43 (d, J = 2.8 Hz), 31.82 (d, J = 32.6 Hz), 29.82 (d, J = 38.3 Hz), 18.00 (d, J = 7.6 Hz), 17.80, 17.08 (d, J = 4.6 Hz), 16.54 (d, J = 3.5 Hz). ^{31}P{^{1}H} NMR (162 MHz, benzene-d_6): δ 142.95. Anal. Calcd for $C_{23}H_{40}ClIrNO_5P$: C, 41.57; H, 6.02; N, 2.15. Found: C, 41.28; H, 5.93; N, 2.09.

Synthesis of [(^{15c5}NCOP^{iPr})Ir(H)][BAr$^F_4$] (2). A 20 mL scintillation vial was charged with 23.2 mg (0.0347 mmol) of **1**, 35.0 mg (0.0404 mmol) of NaBAr$^F_4$, and 6 mL of methylene chloride. The mixture was stirred for 2 h as the color changed from yellow to dark orange. Volatiles were removed in vacuo, and the mixture was dissolved in toluene and filtered through sintered glass. The filtrate was evaporated in vacuo to yield **2** as a dark orange powder (72% yield). Light yellow single crystals suitable for an XRD study were grown by slow vapor diffusion of pentane into a concentrated solution of **2** in toluene at 243 K. ^{1}H NMR (600 MHz, chloroform-*d*): δ 6.78 (t, J = 7.8 Hz, 1H), 6.56 (d, J = 8.0 Hz, 1H), 6.50 (d, J = 7.6 Hz, 1H), 4.48 (d, J = 15.7 Hz, 1H), 4.31−4.07 (m, 5H), 4.01 (t, J = 12.4 Hz, 1H), 3.94 (d, J = 11.0 Hz, 1H), 3.87 (d, J = 12.5 Hz, 1H), 3.80 (d, J = 12.9 Hz, 1H), 3.78−3.71 (m, 2H), 3.62 (td, J = 19.5, 17.0, 10.0 Hz, 3H), 3.56−3.38 (m, 4H), 3.35 (d, J = 13.7 Hz, 1H), 3.05 (d, J = 13.8 Hz, 1H), 2.38 (dt, J = 13.7, 6.8 Hz, 1H), 2.31 (p, J = 7.1 Hz, 1H), 1.29 (dt, J = 13.8, 6.9 Hz, 4H), 1.20 (dd, J = 15.4, 7.2 Hz, 3H), 1.03 (dd, J = 19.8, 7.1 Hz, 3H), 0.94 (dd, J = 16.1, 6.9 Hz, 3H), −30.03 (d, J = 27.2 Hz, 1H). ^{13}C{^{1}H} NMR (151 MHz, chloroform-*d*): δ 163.07, 161.81 (q, $^1J_{BC}$ = 49.9 Hz), 144.64 (d, J = 3.9 Hz), 134.93, 129.07 (q $^2J_{FC}$ = 31.7), 125.25, 124.69 (q, $^1J_{FC}$ = 272.6 Hz), 117.76, 115.46, 108.91, 108.84, 78.44, 74.76, 73.93, 73.38, 70.72, 70.62, 68.65, 68.13, 67.27, 63.05, 60.66, 30.78 (d, $^1J_{PC}$ = 34.2 Hz), 28.90 (d, $^1J_{PC}$ = 41.4 Hz), 17.80, 16.55 (d, $^2J_{PC}$ = 7.6 Hz), 16.47, 16.31 (d, $^2J_{PC}$ = 1.8 Hz). ^{31}P{^{1}H} NMR (162 MHz, chloroform-*d*): δ 141.03. Anal. Calcd for $C_{55}H_{52}BF_{24}IrNO_5P$: C, 44.13; H, 3.50; N, 0.94. Found: C, 44.55; H, 3.60; N, 0.97.

Synthesis of [Li·(OEt$_2$)$_3$][BAr$^F_4$]. A previously reported procedure involving aqueous cation exchange with NaBAr$^F_4$ afforded only the hydrate [Li·(OH$_2$)$_3$][BAr$^F_4$] in our hands.[55] A small-scale alternative procedure was developed to avoid aqueous conditions. In a glovebox a 20 mL scintillation vial was charged with 0.0586 g (0.0579 mmol) of [H·(OEt$_2$)$_2$][BAr$^F_4$] and 5 mL of diethyl ether. The vial was cooled to −78 °C before dropwise addition of 0.044 mL of 1.33 M *n*-butyllithium (0.0586 mmol) with stirring. After the addition, the reaction mixture was warmed to room temperature with stirring. After removal of volatiles in vacuo, the solids were rinsed with pentane and dried under vacuum to afford 0.0530 g of [Li·(OEt$_2$)$_3$][BAr$^F_4$] as a white powder (91% yield). Spectroscopic data were comparable to data obtained from the synthesis by previous methods.

Equilibrium Studies. A Teflon-sealed NMR tube containing 18.0 mg (0.0269 mmol) of (κ^4-^{15c5}NCOP^{iPr})Ir(H)(Cl) (**1**), CDCl$_3$ (0.5 mL), and acetonitrile-^{15}N (0.008 mL, 0.153 mmol) was placed in the NMR probe at 293 K. The probe was cooled at 10 K increments from 293 to 233 K, and the relative concentrations of **1**, *cis*-(^{15c5}NCOP^{iPr})-Ir(H)(Cl)(NCCH$_3$) (**3**), and *trans*-(^{15c5}NCOP^{iPr})Ir(H)(Cl)(NCCH$_3$) (**3′**) were obtained by ^{1}H NMR spectral analysis. Thermodynamic parameters for the conversion of **1** to **3** ($\Delta H°$ = −8.67 kcal mol^{-1}, $\Delta S°$ = −26.63 cal mol^{-1} K^{-1}) were obtained from a van 't Hoff analysis (Figure 4A). Thermodynamic parameters for the conversion of **1** to **3′** ($\Delta H°$ = −8.50 kcal mol^{-1}, $\Delta S°$ = −22.4 cal mol^{-1} K^{-1}) were obtained from a van 't Hoff analysis (Figure 4A). Data tables and NMR spectra are provided in the Supporting Information.

In a Teflon-sealed NMR tube containing 0.430 mL of a stock solution of [(κ^5-^{15c5}NCOP^{iPr})Ir(H)][BAr$^F_4$] (**2**; 0.0322 M in CDCl$_3$) was added 0.0013 mL (0.0419 mmol) of acetonitrile. The tube was sealed and placed in the NMR probe at 293 K. The probe was cooled in 10 K increments from 293 to 243 K, and the relative concentrations of CH$_3$CN, [(κ^4-^{15c5}NCOP^{iPr})Ir(H)(NCCH$_3$)]$^+$ (**5**), and [(κ^3-^{15c5}NCOP^{iPr})Ir(H)(NCCH$_3$)$_2$]$^+$ (**6**) were obtained by ^{1}H NMR analysis. Thermodynamic parameters for the conversion of **5** to **6** ($\Delta H°$ = −7.84 kcal mol^{-1}, $\Delta S°$ = −19.6 cal mol^{-1} K^{-1}) were obtained from a van 't Hoff analysis (Figure 4B). Data tables and NMR spectra are provided in the Supporting Information.

Dihydrogen Activation Reactions. A stock solution of 6.25 mM [(κ^5-^{15c5}NCOP^{iPr})Ir(H)][BAr$^F_4$] (**2**) in CD$_2$Cl$_2$ containing 125 mM Et$_2$O was prepared by dissolving 0.0531 g (0.0355 mmol) of **2** in 5.600 mL of CD$_2$Cl$_2$ and 0.0750 mL (0.7219 mmol) of Et$_2$O. Teflon-sealed NMR tubes were charged with 0.450 mL of the stock solution along with increasing amounts of NaBAr$^F_4$ or of LiBAr$^F_4$. Tubes containing no salts, 0.31 equiv of NaBAr$^F_4$, 1.23 equiv of NaBAr$^F_4$, 1.76 equiv of NaBAr$^F_4$, 2.52 equiv of NaBAr$^F_4$, and 0.40 equiv of LiBAr$^F_4$ were prepared. Initial NMR spectra were taken. The tubes were freeze−pump−thaw degassed twice to remove N$_2$ and back-filled with D$_2$ at 298 K. The reaction progress (**2** to **2-D**) was monitored over time and quantified by integration of the hydride peak relative to the phenyl backbone. To obtain kinetic isotope effect data, reactions were allowed to react for 3 days to ensure complete conversion to **2-D** before being freeze−pump−thaw degassed twice and back-filled with H$_2$. The reaction progress (**2-D** to **2**) was monitored over time by NMR spectroscopy.

The reaction rate could be slowed by addition of chloride. The preceding procedure was followed, with 6.25 mM **2** and 1.94 equiv of NaBAr$^F_4$ under D$_2$ in CD$_2$Cl$_2$. When conversion of **2** to **2-D** had reached 57%, the tube was freeze−pump−thaw degassed. The tube was then charged with 1.76 equiv [NBu$_4$][Cl] under N$_2$. The tube was freeze−pump−thaw degassed twice to remove N$_2$ and back-filled with D$_2$ at 298 K. The reaction was monitored over time by NMR spectroscopy.

Computational Details. All calculations were performed using the Gaussian09 software package.[56] The PBE functional[57] was used for all calculations, with the LANL2DZ basis set[58] and pseudopotential used for Ir and the 6-311G(d,p) basis set[59] used for all other atoms. A slightly truncated ligand set was used, substituting methyl groups for isopropyl groups on the phosphine ligand. Initial geometries were based on the coordinates obtained from X-ray diffraction studies. After optimizing the structure, frequency optimizations were performed for each species to ensure that no imaginary frequencies were present and to compute Gibbs free energy values, which were used throughout. Except as noted, a polarizable continuum model (IEFPCM implemented by Gaussian09) approximated the effects of the CH$_2$Cl$_2$ solvent. Geometric coordinates and the corresponding energy, enthalpy, and entropy values for each optimized structure are available in the Supporting Information. Reaction thermodynamics are also available in the Supporting Information in tabulated and graphical forms.

■ ASSOCIATED CONTENT

Ⓢ Supporting Information

Text, tables, figures, and CIF and xyz files giving NMR spectra, details of kinetic analysis, and computational and crystallographic details. This material is available free of charge via the Internet at http://pubs.acs.org.

AUTHOR INFORMATION

Corresponding Author

*E-mail for A.J.M.M.: ajmm@email.unc.edu.

Notes

The authors declare no competing financial interest.

ACKNOWLEDGMENTS

Acknowledgment is made to the donors of the American Chemical Society Petroleum Research Fund (52325-DNI3) for support of this research. Peter White assisted with X-ray crystallography, and Marc ter Horst assisted with NMR spectroscopy. Sandra E. Spencer and the laboratory of Prof. G. Glish assisted with HRMS experiments. Prof. M. Brookhart and Prof. C. Schauer participated in helpful discussions.

REFERENCES

(1) Jeffrey, J. C.; Rauchfuss, T. B. *Inorg. Chem.* **1979**, *18*, 2658.
(2) Braunstein, P.; Naud, F. *Angew. Chem., Int. Ed.* **2001**, *40*, 680.
(3) Bader, A.; Lindner, E. *Coord. Chem. Rev.* **1991**, *108*, 27.
(4) Vuzman, D.; Poverenov, E.; Shimon, L.; Diskin-Posner, Y.; Milstein, D. *Organometallics* **2008**, *27*, 2627.
(5) Porerenov, E.; Gandelman, M.; Shimon, L.; Rozenberg, H.; Ben-David, Y.; Milstein, D. *Organometallics* **2005**, *24*, 1082.
(6) Oliveri, C. G.; Ulmann, P. A.; Wiester, M. J.; Mirkin, C. A. *Acc. Chem. Res.* **2008**, *41*, 1618.
(7) Lüning, U. *Angew. Chem., Int. Ed.* **2012**, *51*, 8163.
(8) Bassetti, M. *Eur. J. Inorg. Chem.* **2006**, *2006*, 4473.
(9) Slone, C. S.; Weinberger, D. A.; Mirkin, C. A. In *Progress in Inorganic Chemistry*; Karlin, K. D., Ed.; Wiley: Hoboken, NJ, USA, 1999; Vol. *48*, pp 233−350.
(10) Wiester, M. J.; Ulmann, P. A.; Mirkin, C. A. *Angew. Chem., Int. Ed.* **2010**, *50*, 114.
(11) Yoon, H. J.; Kuwabara, J.; Kim, J. H.; Mirkin, C. A. *Science* **2010**, *330*, 66.
(12) Singewald, E. T.; Mirkin, C. A.; Stern, C. L. *Angew. Chem., Int. Ed.* **1995**, *34*, 1624.
(13) Slone, C. S.; Mirkin, C. A.; Yap, G. P. A.; Guzei, I. A.; Rheingold, A. L. *J. Am. Chem. Soc.* **1997**, *119*, 10743.
(14) Allgeier, A. M.; Slone, C. S.; Mirkin, C. A.; Liable-Sands, L. M.; Yap, G. P. A.; Rheingold, A. L. *J. Am. Chem. Soc.* **1997**, *119*, 550.
(15) Przybilla, K. J.; Vögtle, F. *Chem. Ber.* **1989**, *122*, 347−355.
(16) Zhang, X.; Huang, D.; Chen, Y.; Holm, R. H. *Inorg. Chem.* **2012**, *51*, 11017.
(17) Spasyuk, D. M.; Zargarian, D.; van der Est, A. *Organometallics* **2009**, *28*, 6531.
(18) Spasyuk, D. M.; Zargarian, D. *Inorg. Chem.* **2010**, *49*, 6203.
(19) Spasyuk, D. M.; Gorelsky, S. I.; van der Est, A.; Zargarian, D. *Inorg. Chem.* **2011**, *50*, 2661.
(20) Gottker-Schnetmann, I.; White, P.; Brookhart, M. *J. Am. Chem. Soc.* **2004**, *126* (6), 1804.
(21) Kang, P.; Cheng, C.; Chen, Z.; Schauer, C. K.; Meyer, T. J.; Brookhart, M. *J. Am. Chem. Soc.* **2012**, *134*, 5500.
(22) Iglesias, M.; Pérez-Nicolás, M.; Miguel, P. J. S.; Polo, V.; Fernández-Alvarez, F. J.; Pérez-Torrente, J. J.; Oro, L. A. *Chem. Commun.* **2012**, *48*, 9480.
(23) Lindner, E.; Gierling, K.; Fawzi, R.; Steinmann, M. *Inorg. Chim. Acta* **1998**, *269*, 13.
(24) Yamamoto, Y.; Kawasaki, K.; Nishimura, S. *J. Organomet. Chem.* **1999**, *587*, 49.
(25) Dorta, R.; Broggini, D.; Kissner, R.; Togni, A. *Chem. Eur. J.* **2004**, *10*, 4546.
(26) Álvarez, E.; Paneque, M.; Petronilho, A. G.; Poveda, M. L.; Santos, L. L.; Carmona, E.; Mereiter, K. *Organometallics* **2007**, *26*, 1231.
(27) Werner, H.; Schulz, M.; Windmueller, B. *Organometallics* **1995**, *14*, 3659.
(28) Barquín, M.; Ciganda, R.; Garralda, M. A.; Ibarlucea, L.; Mendicute-Fierro, C.; Rodríguez-Diéguez, A.; Seco, J. M. *Chem. Ber.* **2013**, *2013*, 1225.
(29) van Veggel, F. C. J. M.; Verboom, W.; Reinhoudt, D. N. *Chem. Rev.* **1994**, *94*, 279.
(30) Gray, G. M. *Comm. Inorg. Chem.* **1995**, *17*, 95.
(31) Lehn, J.-M. *Pure Appl. Chem.* **1980**, *52*, 2441.
(32) Carroy, A.; Lehn, J.-M. *J. Chem. Soc., Chem. Commun.* **1986**, 1232.
(33) Hazari, A.; Labinger, J. A.; Bercaw, J. E. *Angew. Chem., Int. Ed.* **2012**, *51*, 8268.
(34) Yang, J.; Brookhart, M. *Adv. Synth. Catal.* **2008**, *351*, 175.
(35) Lindner, R.; van den Bosch, B.; Lutz, M.; Reek, J. N. H.; van der Vlugt, J. I. *Organometallics* **2011**, *30*, 499.
(36) Adams, J. J.; Lau, A.; Arulsamy, N.; Roddick, D. M. *Organometallics* **2011**, *30*, 689.
(37) Shi, Y.; Suguri, T.; Dohi, C.; Yamada, H.; Kojima, S.; Yamamoto, Y. *Chem. Eur. J.* **2013**, *19*, 10672.
(38) De Boer, J. A.; Reinhoudt, D. N.; Harkema, S.; Van Hummel, G. J.; De Jong, F. *J. Am. Chem. Soc.* **1982**, *104*, 4073.
(39) Grootenhuis, P. D.; Kollman, P. A. *J. Am. Chem. Soc.* **1989**, *111*, 4046.
(40) Izatt, R. M.; Bradshaw, J. S.; Pawlak, K.; Bruening, R. L.; Tarbet, B. J. *Chem. Rev.* **1992**, *92*, 1261.
(41) These interactions are not accounted for in the DFT model and might affect the values of ΔH substantially. For example, the inclusion of a solvent model (CH_2Cl_2) and an explicit CH_2Cl_2 molecule (hydrogen bonding with a crown ether oxygen atom) led to a decrease in the free energy of ∼2 kcal mol^{-1} and better agreement with the relative energy levels of the isomers (full details in the Supporting Information).
(42) Yakelis, N. A.; Bergman, R. G. *Organometallics* **2005**, *24*, 3579.
(43) Li, D.; Keresztes, I.; Hopson, R.; Williard, P. G. *Acc. Chem. Res.* **2009**, *42*, 270.
(44) Fernandez, I.; Martinez-Viviente, E. S.; Breher, F.; Pregosin, P. S. *Chem. Eur. J.* **2005**, *11*, 1495.
(45) Gibson, H. W.; Yamaguchi, N.; Hamilton, L.; Jones, J. W. *J. Am. Chem. Soc.* **2002**, *124*, 4653.
(46) Heinekey, D. M.; Oldham, W. J. *Chem. Rev.* **1993**, *93*, 913.
(47) Kubas, G. J. *Chem. Rev.* **2007**, *107*, 4152.
(48) Findlater, M.; Schultz, K. M.; Bernskoetter, W. H.; Cartwright-Sykes, A.; Heinekey, D. M.; Brookhart, M. *Inorg. Chem.* **2012**, *51*, 4672.
(49) Izatt, R. M.; Bradshaw, J. S.; Nielsen, S. A.; Lamb, J. D.; Christensen, J. J.; Sen, D. *Chem. Rev.* **1985**, *85*, 271.
(50) Izatt, R. M.; Pawlak, K.; Bradshaw, J. S.; Bruening, R. L. *Chem. Rev.* **1991**, *91*, 1721.
(51) A more detailed interpretation would require comparison to the reaction of **2** with H_2, but this reaction is too slow to study by NMR methods. The observed isotope effect would be consistent with Ir−H/Ir−D bond breaking being involved in the rate-limiting step. Alternatively, equilibrium isotope effects could also contribute to the observed relative rates. For example, D_2 has been shown to be a stronger ligand than H_2, which might manifest itself in the preferential formation of an Ir(H)(D_2) complex. See: Kubas, G. J. *Metal Dihydrogen and σ-Bond Complexes*; Kluwer: New York, 2001.
(52) Fulmer, G. R.; Miller, A. J. M.; Sherden, N. H.; Gottlieb, H. E.; Nudelman, A.; Stoltz, B. M.; Bercaw, J. E.; Goldberg, K. I. *Organometallics* **2010**, *29*, 2176.
(53) Brookhart, M.; Grant, B.; Volpe, A. F., Jr. *Organometallics* **1992**, *11*, 3920.
(54) Dolomanov, O. V.; Bourhis, L. J.; Gildea, R. J.; Howard, J. A. K.; Puschmann, H. *J. Appl. Crystallogr.* **2009**, *42*, 339.
(55) Nishida, H.; Takada, N.; Yoshimura, M.; Sonoda, T.; Kobayashi, H. *Bull. Chem. Soc. Jpn.* **1984**, *57*, 2600.
(56) Frisch, M. J.; Trucks, G. W.; Schlegel, H. B.; Scuseria, G. E.; Robb, M. A.; Cheeseman, J. R.; Scalmani, G.; Barone, V.; Mennucci, B.; Petersson, G. A.; Nakatsuji, H.; Caricato, M.; Li, X.; Hratchian, H. P.; Izmaylov, A. F.; Bloino, J.; Zheng, G.; Sonnenberg, J. L.; Hada, M.;

Ehara, M.; Toyota, K.; Fukuda, R.; Hasegawa, J.; Ishida, M.; Nakajima, T.; Honda, Y.; Kitao, O.; Nakai, H.; Vreven, T.; Montgomery, J. A., Jr.; Peralta, J. E.; Ogliaro, F.; Bearpark, M.; Heyd, J. J.; Brothers, E.; Kudin, K. N.; Staroverov, V. N.; Kobayashi, R.; Normand, J.; Raghavachari, K.; Rendell, A.; Burant, J. C.; Iyengar, S. S.; Tomasi, J.; Cossi, M.; Rega, N.; Millam, N. J.; Klene, M.; Knox, J. E.; Cross, J. B.; Bakken, V.; Adamo, C.; Jaramillo, J.; Gomperts, R.; Stratmann, R. E.; Yazyev, O.; Austin, A. J.; Cammi, R.; Pomelli, C.; Ochterski, J. W.; Martin, R. L.; Morokuma, K.; Zakrzewski, V. G.; Voth, G. A.; Salvador, P.; Dannenberg, J. J.; Dapprich, S.; Daniels, A. D.; Farkas, Ö.; Foresman, J. B.; Ortiz, J. V.; Cioslowski, J.; Fox, D. J. *Gaussian 09, Revision D.01*; Gaussian, Inc., Wallingford, CT, 2009.

(57) Perdew, J. P.; Burke, K.; Ernzerhof, M. *Phys. Rev. Lett.* **1996**, *77*, 3865.

(58) Hay, P. J.; Wadt, W. R. *J. Chem. Phys.* **1985**, *82*, 270.

(59) (a) McLean, A. D.; Chandler, G. S. *J. Chem. Phys.* **1980**, *72*, 5639. (b) Krishnan, R.; Binkley, J. S.; Seeger, R.; Pople, J. A. *J. Chem. Phys.* **1980**, *72*, 650.